ELSEVIER

Polymer 42 (2001) 167–183

polymer

www.elsevier.nl/locate/polymer

Structure–property relationships of irradiation grafted nano-inorganic particle filled polypropylene composites

Min Zhi Rong[a,*], Ming Qiu Zhang[a], Yong Xiang Zheng[a], Han Min Zeng[b], R. Walter[c], K. Friedrich[c]

[a]*Materials Science Institute, Zhongshan University, Guangzhou 510275, People's Republic of China*
[b]*Key Laboratory of Polymeric Composite and Functional Materials, The Ministry of Education of China, Zhongshan University, Guangzhou 510275, People's Republic of China*
[c]*Institute for Composite Materials (IVW), University of Kaiserslautern, D-67663 Kaiserslautern, Germany*

Received 15 November 1999; received in revised form 21 March 2000; accepted 18 April 2000

Abstract

An irradiation grafting method was applied for the modification of nanoparticles so that the latter can be added to polymeric materials for improving their mechanical performance, using existing compounding techniques. The following items are discussed in particular, in this paper: (a) chemical interaction between the grafting monomers and the nanoparticles during irradiation; (b) properties including modulus, yield strength, impact strength and fracture toughness of the resultant nanocomposites; and (c) possible morphological changes induced by the addition of nanoparticles. Through irradiation grafting polymerization, nanoparticle agglomerates turn into a nano-composite microstructure (comprising the nanoparticles and the grafted, homopolymerized secondary polymer), which in turn builds up a strong interfacial interaction with the surrounding, primary polymeric matrix during the subsequent mixing procedure. Due to the fact that different grafting polymers brought about different nanoparticle/matrix interfacial features, microstructures and properties of the ultimate nanocomposites could thus be tailored. It was found that the reinforcing and toughening effects of the nanoparticles on the polymer matrix could be fully brought into play at a rather low filler loading in comparison to conventional particulate filled composites. Unlike the approaches for manufacturing of the other types of nanocomposites, including intercalation polymerization, the current technique is characterized by many advantages, such as simple, low cost, easy to be controlled and broader applicability.

Keywords: Nanocomposites; Polypropylene; Toughening and strengthening

1. Introduction

The incorporation of inorganic particulate fillers has been proved to be an effective way for the improvement of the mechanical properties, and in particular the toughness, of polymeric materials. However, the typical filler contents needed for such an enhancement of performance are as high as 20% by volume [1,2]. As a result of this high particle loading, the processability of the compounds is inevitably deteriorated and the weight of the end-products becomes much higher than that of the neat polymers; this limits various applications of these materials in transportation subsegments, in the electrical and electronic industry, and in the appliance and equipment industry. The basic advantages of polymers, i.e. their ease of processing and lightweight, get therefore lost. That means, a composite with improved properties and lower particle concentration is highly desired. With regard to this, the newly developed nanocomposites would be competitive candidates.

Polymer based nanocomposites are attracting considerable attention owing to their unique properties resulting from the nano-scale microstructure; the latter is characterized by the large fraction of filler atoms that reside at the surface of the nanoparticles and that lead to strong interfacial interactions with the surrounding polymer matrix. In case the ultra-fine phase dimensions of the nanoparticles are maintained after compounding with a particular polymer matrix, such nanocomposites will possess a significant improvement in both rigidity and toughness at a filler content far less than it can be achieved in comparable glass or mineral reinforced polymers. As such they are much lighter in weight, transparent and easier to be processed than conventional inorganic particulate filled polymers [3].

* Corresponding author. Tel.: +86-20-84039053; fax: +86-20-84036564.
E-mail address: cesrmz@zsulink.zsu.edu.cn (M.Z. Rong).

0032-3861/01/$ - see front matter
PII: S0032-3861(00)00325-6

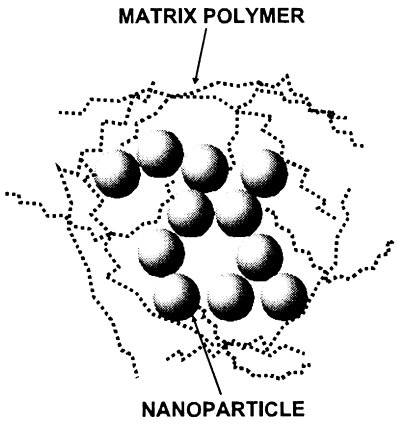

Fig. 1. Agglomerated nanoparticles dispersed in a polymer matrix.

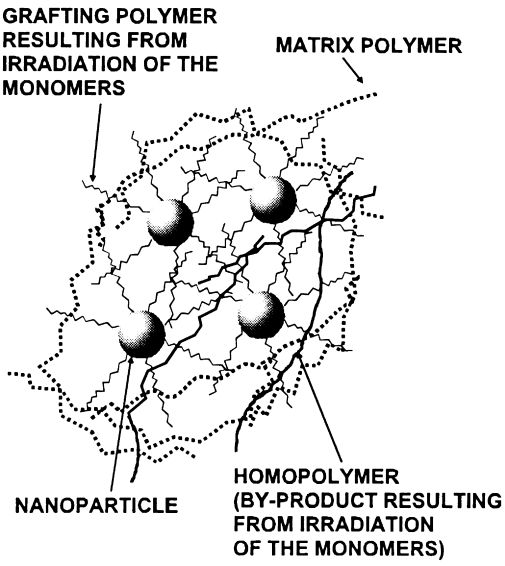

Fig. 2. Schematic drawing of the possible structure of grafted nanoparticles dispersed in a polymer matrix.

However, a homogeneous dispersion of nanoparticles in a polymeric matrix is a very difficult task due to the strong tendency of nanoparticles to agglomerate. Consequently, the so-called nanoparticle filled polymers sometimes contain a number of loosened clusters of particles (Fig. 1) and exhibit properties even worse than conventional particle/polymer systems. To break down these nanoparticle agglomerates and to produce nanostructural composites, many researchers focus on the approaches of in-situ polymerization of monomers in the presence of nanoparticles, such as the sol–gel process [4] and the intercalation polymerization technique [5]. These methods utilize kinetic and thermodynamic controls. During the sol–gel process, for example, polymers can be kinetically trapped within inorganic matrices under the right set of conditions prior to significant phase separation. Clay layer exfoliation is regulated by mediating diffusion and polymerization of monomers to the galleries. The thermodynamic control is governed by the hydrophobicity of the organoclays, which plays an important role in allowing monomer molecules to migrate into the clay gallery region. Although nano-scale dispersion of the particles can be obtained accordingly, these methods, characterized by complex polymerization and special conditions, are not applicable to most of the technically important polymers because neither a suitable monomer nor a compatible polymer–silicate solvent system is always available. In addition, most nanoparticles are non-layered inorganic substances. Evidently, a mass production of nanocomposites with cost effectiveness and applicability has to follow another route.

By examining the current technical level and the feasibility of the available processing methods, it can be concluded that the widely used compounding techniques for the preparation of conventionally filled polymers is still the most convenient way when nanoparticles are proposed to replace the micron-scale fillers for the purposes of performance enhancement without variation of processability and density of the resultant composites. The problem is that nanoparticle agglomerates are also hard to be disconnected by the limited shear forces in polymer melts characterized by a high viscosity during melt mixing. This is true even when a coupling agent is used [6]. Since the latter can only react with the exterior nanoparticles, the agglomerates will maintain their friable structure in the composite and can neither provide reinforcing nor toughening effects [7]. On the contrary, when more nanoparticles are added, the tensile yield strength becomes lower due to an increased probability of breaking and splitting of the agglomerated nanoparticles [8,9]. Similarly, such kinds of nanocomposites do not resist crack propagation under higher speed load as effectively as matrix resins, thus exhibiting reduced impact strength values [10].

Based on these results, we can infer that it might be impossible to pursue a nano-scale dispersion of the particles, especially when considering the high viscosity of the polymer melt as well as the poor interaction between the hydrophilic fillers and the hydrophobic matrix. Besides the dispersion status promotion, a lot of emphasis should be focussed on the modification of the agglomerates themselves by means of a special surface treatment of the nanoparticles.

In this paper, a combination of in-situ polymerization and mechanical compounding is developed to overcome the defects existing in the above-mentioned methods. The key issue is that the nanoparticles are modified by irradiation graft polymerization first, and then the grafted nanoparticles are mechanically mixed with a polymer as usual. Owing to the low molecular weight nature, the grafting monomers can penetrate into the agglomerated nanoparticles easily and react with the activated sites of the nanoparticles inside as well as outside the agglomerates. Nanocomposites with a distinct structure (Fig. 2) would thus be obtained due to the

following effects:

1. An increase in hydrophobicity of the nanoparticles due to the grafting polymers would be beneficial for the filler/matrix miscibility even if a completely uniform distribution of the particles cannot be achieved during the subsequent compounding.
2. The filler/matrix interaction would be substantially enhanced by the entanglement between the grafting polymer and the main polymer matrix.
3. The nanoparticle agglomerates would become much stronger because they turn into a nano-composite microstructure comprising the nanoparticles and the grafted, homopolymerized secondary polymer.
4. As different grafting polymers might bring about different interfacial characteristics between the modified nanoparticles and the main polymer matrix, the structure–property relationships of these nanocomposites could be tailored by changing the species of the grafting monomers and the grafting conditions. In this case, a uniform dispersion of primary nanoparticles in the matrix, as desired usually, might no longer be critical.

The purpose of this paper is to show how efficiently the mechanical performance of the nanocomposites can be improved by the above approach and the related microstructural variation. Polypropylene (PP) and nano-silica (SiO_2) were chosen as the matrix and the filler for the nanocomposites production, respectively, partly because of the practical importance of these materials and the extensive information available related to the conventional SiO_2-particles filled PP. Chemical interaction between the monomers and the nanoparticles during the irradiation procedure, mechanical performance of the nanocomposites, and possible morphological changes induced by the addition of the nanoparticles are discussed in detail.

2. Experimental

2.1. Materials

General-purpose isotactic PP homopolymer (type F401, melting flow index (MI) = 8.5 and 6.7 g/10 min, respectively) provided by Guangzhou Petroleum Chemical Co., China, was used as matrix in this work. The nanoparticles consist of pyrogenic colloidal SiO_2 (Aerosol 1380, Degussa Co., Germany) with an average primary particle size of 7 nm and a specific gravity of 2.2 g/cm^3. Commercial monomers: styrene, methyl methacrylate, butyl acrylate, ethyl acrylate, methyl acrylic acid and vinyl acetate, were used as grafting monomers without further purification.

2.2. Pregrafting of the nanoparticles by irradiation

The typical pregrafting of SiO_2 proceeded as follows. Before being mixed with the monomers, the nanoparticles were preheated at 120°C for 5 h to eliminate possible absorbed water on the surface of the particles. Then the mixture of monomer/particles (20/100 by weight) and a certain amount of solvent (heptane, or acetone, or ethanol, depending on different monomer/SiO_2 systems) was irradiated by ^{60}Co γ-ray under atmosphere at a dose rate of 1 Mrad/h at room temperature. After exposure to a dose of 30 Mrad, the solvent was recovered, and the dried residual powder could be compounded with the thermoplastic matrix directly (see later).

As the structure of the irradiation products is a function of irradiation conditions, which might then lead to great effects on the structure and properties of the nanocomposites, parameters including irradiation dose, pretreated temperature and content of monomer were changed to study their influence on the mechanical properties of the nanocomposites.

2.3. Characterization of irradiation products and interaction between nanoparticles and grafting polymers

To measure molecular weights of the grafting polymer and the homopolymer, which are simultaneously derived from irradiation polymerization of the monomers, and to characterize the interaction feature on the surface of the particles as well, the grafting polymer and homopolymer should be separated. For this purpose, certain amounts of the irradiation products were extracted with solvents (benzene for polystyrene, acetone for polymethyl methacrylate, polybutyl acrylate, polyethyl acrylate and polyvinyl acetate, methanol for polymethyl acrylate, respectively). This procedure for which a Sohnley apparatus was used lasted over 37 h; the residual material was then dried under vacuum for 5 h at 80°C. In this way, homopolymers were selectively separated from the irradiated powder. The weight increase in SiO_2 due to the presence of unextractable polymers (i.e. the grafting polymers) was then determined by weighing and thermogravimetric analysis (TGA, Shimadzu TA-50 thermogravimetre). It was found that the results given by the two methods agree well within experimental errors. In a second step, SiO_2 accompanied with the unextractable grafting polymer was immersed in 10–20% HF solution for 1–2 days to remove the SiO_2 particles, so that the grafting polymer could be recovered finally. Based on these procedures, the molecular weights of both the grafting and the homopolymerized polymers were measured by using Waters 208LC gel permeation chromatography (GPC), with chloroform as the solvent at room temperature. Escalab ZZOI-XL electron spectroscopy for chemical analysis (ESCA) and a Nicolet 5DX Fourier transform infrared spectroscope (FTIR) were also utilized to characterize changes in the nanoparticle surfaces and in the molecular structure of the grafted polymers.

As a reference, SiO_2 was coated with PS by solution blending in benzene, then precipitated by centrifugation and dried in vacuum. TGA and Hitachi H-800 transmission electron microscopy (TEM) were used to compare the

Table 1
Percent grafting and grafting efficiency of styrene/SiO_2 system as a function of irradiation conditions

Weight ratio of styrene/SiO_2	Preheating temperature (°C)	Irradiation dose (Mrad)	Monomer conversion[a] (%)	Percent grafting[b] (%)	Grafting efficiency[c] (%)
20/1	120	2	0.84	0.84	33.9
20/1	120	4	1.20	1.20	24.7
20/1	120	8	5.02	5.02	9.4
10/1	500	10	39.1	17.3	3.7
3/1 (at the presence of heptane)	500	10	43.0	10.5	7.2

[a] Monomer conversion = weight of polymer/weight of monomer.
[b] Percent grafting = weight of grafting polymer/weight of SiO_2.
[c] Grafting efficiency = weight of grafting polymer/weights of grafting polymer and homopolymer.

thermal and dispersion stability of the PS coated SiO_2 in the solvent with the corresponding values of the PS grafted SiO_2. The TEM samples were prepared from benzene dispersion of the particles, which were deposited on a copper grid covered with a carbon film prior to the observation.

2.4. Preparation of nanocomposites and their characterization

Nanocomposites were prepared by tumble mixing the preweighted quantities of PP and grafted fillers first, followed by compounding this mixture on a lab-scale single screw extruder. The manufacturing temperature was kept at 200°C and the screw speed amounted to 25 rpm. The specimens for mechanical tests were machined from compressing molded plates ($65 \times 45 \times 3\ mm^3$) of the extrudates. The volume fraction of the fillers could be computed from the known weights of the polymer matrix, the fillers and the polymer introduced by irradiation. The TEM examination was performed on ultrathin sections of the nanocomposites. The examination of the reinforcing efficiency of the nanoparticle agglomerates took place by measurement of the parameters Young's modulus, tensile yield strength, impact strength and fracture toughness. Tensile tests were carried out on dumbbell shaped specimens by a LWK-5 universal testing machine at a crosshead speed of 10 mm/min. A XJJ-5 tester was used for unnotched Izod and Charpy impact strength measurements. Fracture toughness determination of the samples followed the ASTM 5045-93, using single edge notched bending (SENB) specimens at a crosshead speed of 5 mm/min. The fractured surfaces were studied by a HITACHI S-520 scanning electron microscope (SEM).

Melting and crystallization behavior of PP and its nanocomposites were examined in N_2 by differential scanning calorimetry (Perkin–Elmer DSC 7C). For non-isothermal measurements, both the heating and cooling rates were 10°C/min. For isothermal tests, the samples were heated up to 210°C at 10°C/min, kept for 5 min, and they were then cooled to the desired crystallization temperatures of 130 or 132°C as quickly as possible.

The influence of nanoparticles on the flow behavior of PP was evaluated using a computer controlled torque rheometer Haake Rheocord 90 (temperature: 190°C, rotor speed: 50 rpm, sample weight: 50 g).

3. Results and discussion

3.1. Effect of irradiation conditions and characterization of interactions between nanoparticles and grafting polymers

Nanoparticles possess properties which are quite different from those estimated from the particles of conventional size; these differences are due to size effects, interfacial effects, and structural defects. Since there is not much information available about irradiation grafting reaction of polymers on nanoparticles, some important irradiation parameters, such as irradiation dose, effect of solvent and preheating temperature, should be identified at the very beginning.

Table 1 lists the experimental data of a styrene/SiO_2 system as an example. It can be seen that the conversion and percentage of grafting of styrene increase as the irradiation dose increases, while the grafting efficiency decreases. This phenomenon indicates that a higher irradiation dose can produce more activated sites for homopolymerization than for grafting reactions, in spite of the fact that an increase in either of the reactions contributes to an increase in monomer conversion.

As nanoparticles have higher surface activity, strict irradiation grafting conditions, such as high vacuum and purification of monomers which are usually required in the case of conventional particles, are no longer necessary. To iron out the differences caused by monomer diffusion and to ensure sufficient wetting to each of the nanoparticles, a larger amount of monomers (styrene/SiO_2 = 20/1) was used in the absence of solvents. However, styrene conversion remains at a rather low level in the irradiation dose range of 2–8 Mrad (Table 1). Considering the fact that a higher irradiation dose and less monomer in the presence of a specific solvent (for good contact with the particles) facilitate a higher conversion rate, the irradiation dose was increased to 10 Mrad, and the weight ratio of styrene/SiO_2 was reduced to 10/1–3/1. The data in Table 1 suggest that

Table 2
Grafting details of SiO_2 grafted with different polymers (irradiation dose = 10 Mrad; weight ratio of monomer/SiO_2 = 20/100; all the systems used acetone as solvent when they were irradiated, except for methyl acrylic acid/SiO_2 system with ethanol as solvent)

Grafting polymers	PS[a]	PBA[b]	PVA[c]	PEA[d]	PMMA[e]	PMA[f]
Percent grafting (%)	3.64	3.32	2.82	1.73	1.85	2.16
Homopolymer fraction[g] (%)	16.3	15.4	13.7	12.3	15.5	15.4

[a] PS = polystyrene.
[b] PBA = polybutyl acrylate.
[c] PVA = polyvinyl acetate.
[d] PEA = polyethyl acrylate.
[e] PMMA = polymethyl methacrylate.
[f] PMA = polymethyl acrylate.
[g] Homopolymer fraction = weight of homopolymer/weight of SiO_2.

the method works, especially when heptane is associated. A further decrease in the monomer fraction can even result in almost a 100% conversion as shown in Table 2 (for example, in the case of the styrene/SiO_2 system, the relative percentage of the grafting plus homopolymer fraction approximately equals 20/100, i.e. the weight ratio of styrene/SiO_2 prior to the irradiation treatment). In addition, the rise in grafting efficiency in the presence of heptane, as shown in Table 1, implies that the solvent impeded the formation of the homopolymer probably due to the effect of chain transfer. Therefore, in the present work a reaction system with a proper solvent is chosen as a typical condition.

As a kind of pyrogenic colloidal silica, the surface of SiO_2 generally contains 5–10 wt% absorbed water which might interrupt the contact of monomers with SiO_2. However, in the case of conventional micron-scale particles, the absorbed water can be almost completely removed by heat treatment at 120–130°C [11]. On heating above 120°C, the dehydration of silanol groups on the SiO_2 surface takes place gradually, leading to a declined reaction activity of the particles. When the treatment temperature exceeds 500°C, the structure of SiO_2 starts to change from an amorphous to a crystalline one and its specific surface area diminishes stepwisely. Consequently, the percentage of grafting would decrease with increasing preheating temperature, with monomer conversion being equal. In contrast to this tendency, the current nano-SiO_2/system exhibits a higher percentage of grafting when the SiO_2 was heated at 500°C (Table 1), which must be related to a higher surface activity of the nanoparticles in this case. Even at a temperature as high as 500°C, the dehydration of silanol groups was not significant due to the high absorption feature of the nanoparticles surface. The phenomenon of the relatively wide preheating temperature window can also be perceived from the impact tests of the nanocomposites (see Section 3.3). That is, no differences in impact strength were detected within a preheating temperature range between 120 and 500°C. Therefore, a low temperature treatment at 120°C was applied to nano-SiO_2 in this work for energy saving.

The number average molecular weight, M_n, and weight average molecular weight, M_w, of both grafting and homopolymerized polystyrene obtained by irradiation are shown in Table 3. The larger M_n of the homopolymer than that of the grafting polymer could be ascribed to the higher mobility of the nanoparticles compared with conventional particles, which made chain termination between radicals easier. Besides, a wider distribution of the molecular weight of PS in the system with heptane should be a result of chain transfer from the radicals to the solvent.

Fig. 3 shows the infrared spectra of SiO_2 as-received, SiO_2-*g*-PS, grafting PS and homopolymerized PS. The latter two polymers were isolated from the irradiation product of styrene/SiO_2. In the spectrum of SiO_2-*g*-PS, there are absorption peaks at 700 and 1400–1600 cm^{-1}, which are characteristic of PS. The most interesting outcome is the appearance of a hydrogen bond peak in the spectrum of grafting PS (at a wavenumber of 3500 cm^{-1}), which is absent in the spectrum of the PS homopolymer, indicating the existence of Si–O–C bonds. This is because the grafting PS for the FTIR measurement was obtained by removing the SiO_2 particles in SiO_2-*g*-PS (in which the homopolymerized PS had already been extracted, see Section 2) with HF solution, the hydrogen bond revealed here can only be the result of the breakage of the Si–O–C bond during the above corrosion procedure. Otherwise, PS with –OH end groups (PS–OH) would not be found. In other words, styrene had reacted with silanol groups of SiO_2 under the circumstances of irradiation. Fig. 4(a) shows the C1s spectrum of PS coated SiO_2, which consists of two components at 285.1 and 282.3 eV representing C–C or C–H and an aromatic ring, respectively. In the case of SiO_2-*g*-PS (Fig. 4(b)), two additional peaks appear, reflecting the chemical interaction between SiO_2 and the grafting polymers. The appearance of the high binding energy (BE) peak reveals that some carbon atoms become electron-poorer after PS is grafted on the surface of SiO_2. If bonds of Si–O–C were present, the ether oxygen atom would have a strong electron-withdrawing effect on the carbon atoms of PS, resulting in a decrease in the electron density of the PS chains. On the other hand, the appearance of a low BE peak can be attributed to the formation of Si–C bonds which made the attached carbon atoms electron-rich. The corresponding variation in the

Table 3
Molecular weights of grafting PS and homopolymerized PS in SiO_2-*g*-PS (SiO_2-*g*-PS means SiO_2 grafted with PS; preheating temperature = 500°C; irradiation dose = 10 Mrad)

Materials	$M_w \times 10^4$	$M_n \times 10^4$	M_w/M_n
Grafting PS[a]	3.5	1.7	2.1
Homopolymerized PS[a]	7.3	4.3	1.7
Grafting PS[b]	5.3	2.2	2.4
Homopolymerized PS[b]	2.1	6.3	3.3

[a] Solvent was absent during the irradiation treatment; weight ratio of monomer/SiO_2 = 10/1.
[b] Heptane was present during the irradiation treatment; weight ratio of monomer/SiO_2 = 3/1.

electron structure of Si is shown in Fig. 5, where the electron-poor Si in SiO_2-*g*-PS results in a shift of the Si2p peak towards a high BE regime as compared with that of SiO_2 as-received. In addition, the peak position increases with a rise in the irradiation dose, indicating that more silicon atoms can be activated by a higher irradiation dose. To conclude, it can be ruled out here that PS is chemically connected with SiO_2 through the Si–O–C and Si–C bonds due to the effect of irradiation grafting.

The structural difference between SiO_2/PS systems with and without chemical bonding between nanosilica and PS actually results in different thermal stabilities, as demonstrated by TGA tests (Fig. 6). It can be roughly estimated from the curves that the temperature corresponding to the maximum weight loss rate of SiO_2-*g*-PS is over 30°C higher than that of PS coated SiO_2.

To look into the structural characteristics of the pre-grafted nanoparticles from another angle, the stability of dispersion of SiO_2-*g*-PS in benzene (a good solvent for PS) was compared with that of PS coated SiO_2 in benzene and SiO_2 as-received in water, respectively. The untreated SiO_2 completely precipitated within one day, while the SiO_2-*g*-PS/benzene solution was transparent for several days. TEM observations (Fig. 7) reveal that the PS physically absorbed on the silica scarcely contributes to the improvement of the particles' dispersiveness, but SiO_2-*g*-PS gives a stable colloidal dispersion in benzene. It manifests that the grafting polystyrene chains on the surface of the nanoparticles interfere with the agglomeration of the particles as shown in Fig. 7(c).

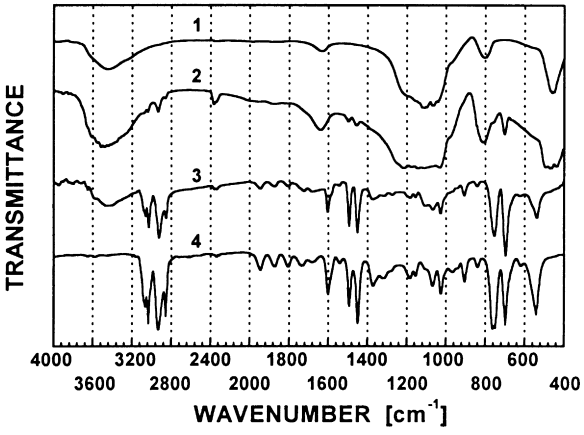

Fig. 3. FTIR spectra of: (1) SiO_2 as-received; (2) SiO_2-*g*-PS; (3) grafting PS; and (4) homopolymerized PS.

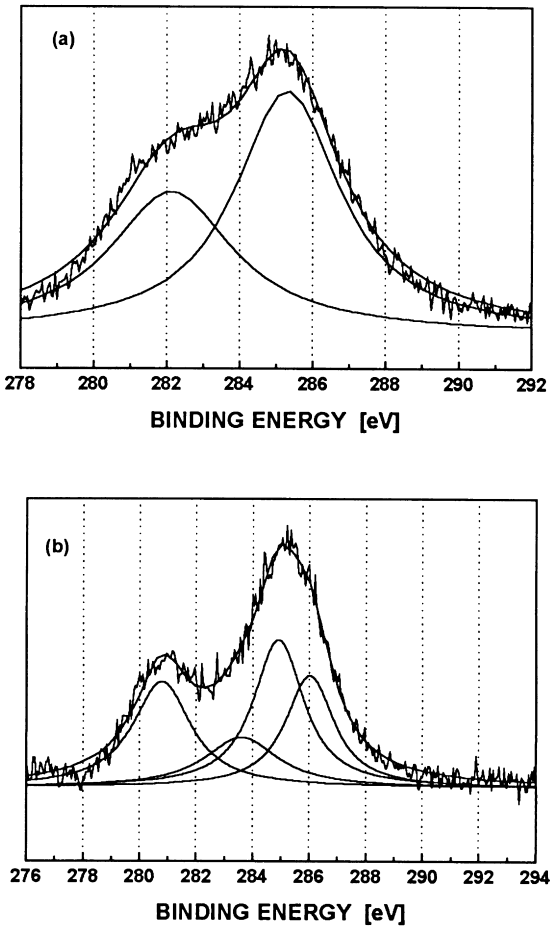

Fig. 4. C1s spectra of: (a) PS coated SiO_2; and (b) SiO_2-*g*-PS.

It can be expected that the above specific features of polymer grafted nano-SiO_2 will also be beneficial for the interfacial interactions between the modified particles and the matrix polymer during the subsequent nanocomposites manufacturing procedure.

3.2. Tensile properties of the nanocomposites

Typical tensile stress–strain curves of neat PP and its filled version are shown in Fig. 8, indicating that both a reinforcing and a toughening effect of the nanoparticles on the polymeric matrix was fully brought into play, as expected from the introductory part of this paper. That is, a structural weakness that would have resulted from the agglomerating behavior of the nanoparticles has been fully eliminated by the grafting macromolecular chains.

By examining the composition-dependent tensile properties of the materials (Fig. 9), it can be seen that the

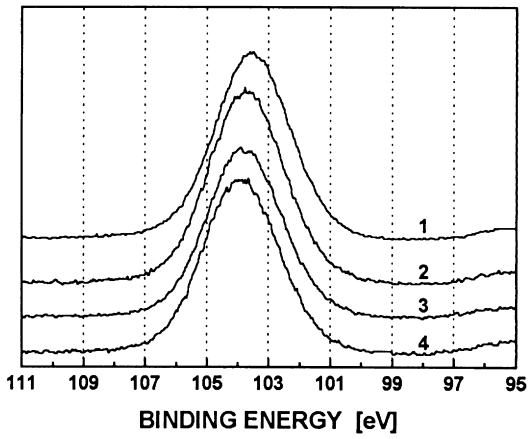

Fig. 5. Si2p spectra of: (1) SiO_2 as-received; (2) SiO_2-*g*-PS (irradiation dose = 2 Mrad); (3) SiO_2-*g*-PS (irradiation dose = 4 Mrad); and (4) SiO_2-*g*-PS (irradiation dose = 8 Mrad).

incorporation of untreated nano-SiO_2 lowers the tensile strength of PP in the lower loading region, but then leads to a slight increase in strength when the particle fraction reaches 4.68 vol% (Fig. 9(a)). When the nanocomposites are filled with PS or PMMA grafted SiO_2, however, the situation is quite different. When there is a considerable rise in the strength of SiO_2-*g*-PS/PP composites at a SiO_2 content as low as 0.65 vol%, then the strength remains almost unchanged with a further addition of the filler. Similar behavior can be observed in the case of SiO_2-*g*-PMMA/PP, except that a slight drop in strength occurs when the filler content exceeds 1.96 vol%. Nevertheless, compared to the untreated case, it can be stated here that mechanical loading seems to be more effectively transferred from the matrix to the filler particles owing to the interfacial bonding effect of the grafting polymers, which might result in an interdiffusion and entanglement between the molecules of the grafting polymers and the matrix. The decrease in tensile strength of SiO_2-*g*-PMMA/PP above 1.96 vol% can be interpreted by a change in the dispersion status of the fillers. It is believed that a higher filler loading is detrimental to its

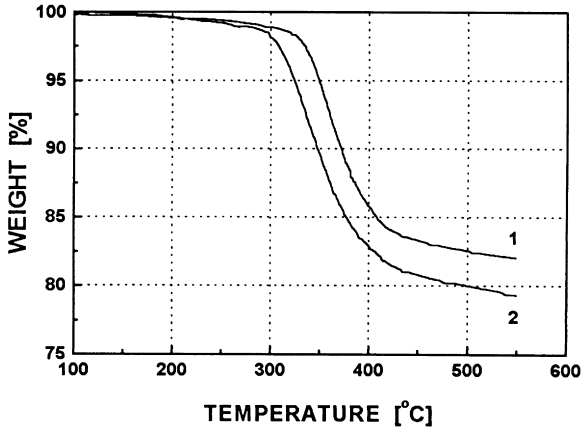

Fig. 6. Thermogravimetric analysis of (1) SiO_2-*g*-PS in comparison with (2) PS coated SiO_2.

uniform dispersion in the polymer matrix. In fact, the TEM observation showed that the size of the dispersed phases increases with increasing filler content in the nanocomposites (Fig. 10). It should be noted here that the dispersed phases in the nanocomposites illustrated in Fig. 10(b)–(e) are clearly smaller than the untreated SiO_2 (Fig. 10(a)), but they are still much larger than the size of the primary nano-SiO_2 particles (7 nm). Therefore, these dispersed phases are actually microcomposite agglomerates consisting of primary particles, grafting polymer, homopolymer, and a certain amount of matrix.

It is well known that the interface adhesion markedly influences the mechanical behavior of particulate filled polymer composites [12–17]. The present irradiation grafting pretreatment provides possibilities for interfacial design, i.e. both surface characteristics of the nanoparticles and the particle agglomerates/matrix interface can be changed by using different grafting monomers. Consequently, the mechanical properties of the nanocomposites can be tailored accordingly. Table 4 gives the mechanical properties of nanocomposites filled with SiO_2 particles, grafted with various polymers, at a fixed SiO_2 fraction. Although the monomers of the grafting polymers should have different miscibilities with PP, all the grafting polymers except PEA exhibit a reinforcement effect on the tensile strength of the nanocomposites. These results contribute to a further understanding of the modified nanoparticles and their role in the composites. That is, interdiffusion and entanglement of the grafting polymer segments with the PP molecules, instead of a miscibility between the grafting polymer and the matrix, dominate the interfacial interaction in the nanocomposites. This leads to the conclusion that a PP matrix with a higher molecular weight should be entangled more effectively with the nanoparticles agglomerates, thus leading to a higher tensile strength increment (comparing Fig. 8 with Table 4). In fact, Kendall and Sherliker [18] studied the effect of the polymer molecular weight on colloidal silica filled thermoplastics and observed a similar phenomenon.

For the moment, it can be concluded that the reinforcing effect of nanoparticles on the polymeric matrices can be realized as long as the particles are grafted and a proper dispersion of the modified particles can be formed. Besides, the tensile properties of the nanocomposites can be purposely adjusted according to the interfacial viscoelastic properties provided by different grafting monomers.

As a parameter closely related to the static stress transfer at the interface, Young's moduli of the composites show another aspect of the role played by the grafting polymers, or rather by the interphase related to them (Table 4). The increase in stiffness of the nanocomposites is obviously a result of the high modulus of the particulate fillers ($modulus_{silica} = 70$ GPa). However, considering that the tensile modulus was determined within only a small strain range (where Hooke's law is still valid), the formation of a relatively compliant layer at the interface (PBA, PVA and PEA, for example) tends to hinder a complete stress transfer

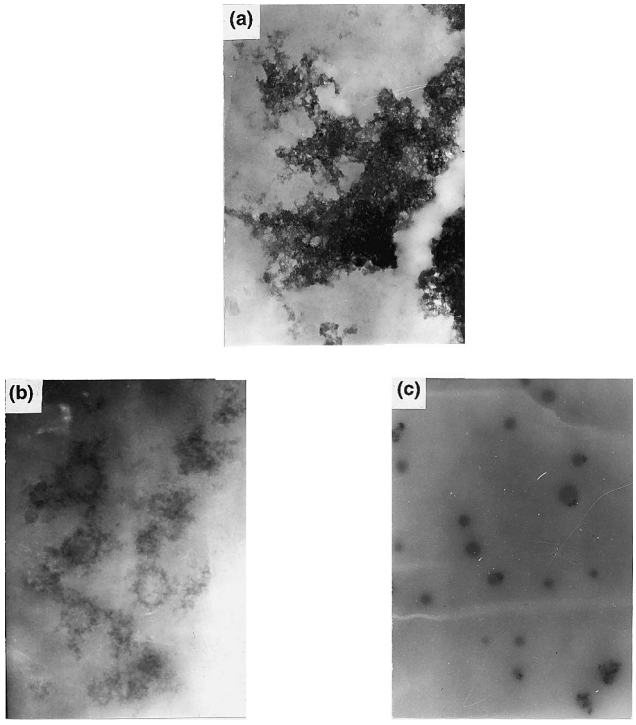

Fig. 7. TEM micrographs of: (a) SiO_2 as-received, magnification $= 2 \times 10^4$; (b) PS coated SiO_2, magnification $= 3 \times 10^4$; and (c) SiO_2-*g*-PS, magnification $= 2 \times 10^4$.

under such a low stress level and thus masks the stiffness of the filler particles. Fig. 9(b) gives an evidence of this mask effect of the grafting polymers, revealing that the modulus of the composites filled with untreated SiO_2 increases almost linearly with the addition of SiO_2, while grafting PS and PMMA greatly decrease the stiffening effect of SiO_2. Walter and co-workers obtained similar results in differently treated Kaolin/high density polyethylene systems [19].

The elongation-to-break of the nanocomposites exhibits a more complicated relationship to the interfacial characteristics in the case of a lower molecular weight PP matrix (Table 4). Relative to the neat matrix, the values of the grafting polymer treated, particle reinforced nanocomposites remain on the same level, except for the PEA treated system. For the matrix with the higher molecular weight (Fig. 9(c)), however, the filler content dependence of the elongation-to-break seems to be clearly evident. The reduction in elongation-to-break of the composite by the addition of untreated SiO_2 implies that the fillers cause a reduction in matrix deformation due to an introduction of mechanical restraints. When the nanoparticles are grafted with PS and PMMA, on the other hand, an increase in elongation-to-break can be found because both interfacial viscoelastic deformation and matrix yielding can contribute to this value. The further tendency of a decrease in elongation-to-break above a filler content of about 1.96 vol% suggests that matrix deformation is not only related to the interface feature but also to the dispersion state of the fillers.

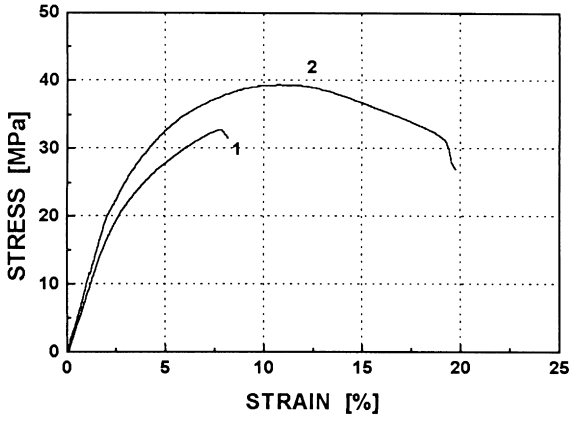

Fig. 8. Typical tensile stress–strain curves of: (1) the neat PP matrix resin (MI = 6.7 g/10 min); and (2) the one filled with SiO_2-*g*-PS (content of $SiO_2 = 1.96$ vol%).

Compared with elongation-to-break, the area under the tensile stress–strain curve is able to more reasonably characterize the toughness potential of the nanocomposites under static tensile loading circumstances. From the data in Table 4, it can be seen that the addition of modified nano-SiO_2 helps to improve the ductility of the PP, except in the case of SiO_2-*g*-PEA. It is believed that localized plastic deformation or drawing of the matrix polymer, being the main energy absorption process in particulate filled polymer systems, can be induced more efficiently by SiO_2-*g*-PS and SiO_2-*g*-PMMA than by untreated SiO_2 (Fig. 9(d)). The deteriorated effect of grafting PEA on the tensile behavior of the nanocomposites cannot be explained by the present results, i.e. further detailed studies have to be carried out.

The above discussion is focussed mainly on the effects of modified SiO_2 due to the presence of grafting polymers. In fact, the internal structure of the grafted nanoparticles also plays an important role in determining the mechanical properties of the nanocomposites. It can be assumed that the molecular weight, the branching degree and the content of both the grafting polymer and the homopolymer around the modified nanoparticles are closely related to the stress distribution of the dispersed phases in the nanocomposites. As shown in Table 5, both tensile strength and elongation-to-break of the nanocomposites decrease with a rise in the irradiation dose from 2 to 20 Mrad, due to a possible cross-linked structure of PS as a result of over-irradiation. A uniform dispersion of the grafted nanoparticles in the polymer matrix would thus be obstructed during the compounding process. Table 6 demonstrates that the area under the tensile stress–strain curve of the nanocomposites decreases with an increasing amount of styrene; this can be considered as an indication of the importance of the arrangement of primary SiO_2 particles inside the grafted agglomerates.

In short, the distribution of nanoparticles in the dispersed phases and that of the dispersed phases in the nanocomposites greatly affect the mechanical properties of

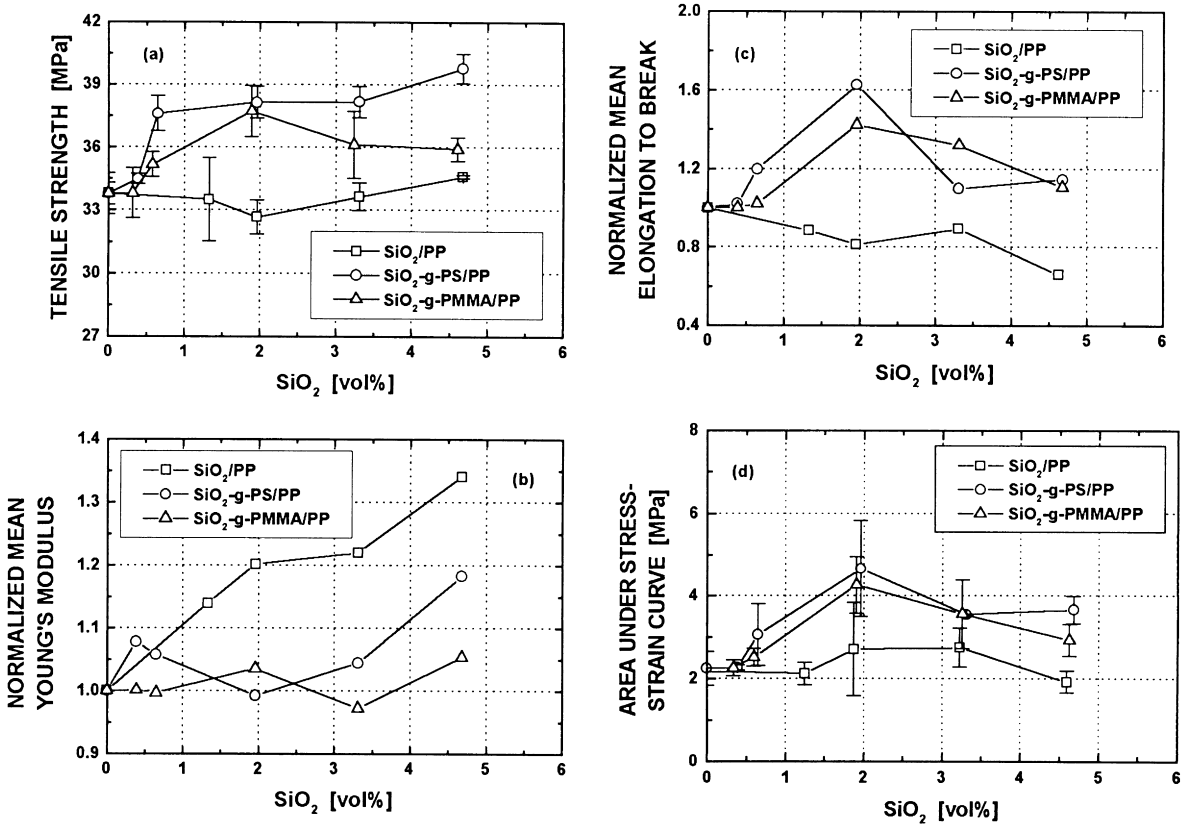

Fig. 9. Tensile properties of PP (MI = 6.7 g/10 min) based nanocomposites as a function of SiO_2 content: (a) tensile strength; (b) normalized mean Young's modulus; (c) normalized mean elongation-to-break; and (d) area under stress–strain curve.

nanocomposites, which should be fully considered when designing novel nanocomposites.

3.3. Impact resistance and fracture toughness of the nanocomposites

Fig. 11 illustrates the effects of untreated SiO_2 and polymer-grafted SiO_2 particles on the unnotched Izod impact strength of PP. Both PS and PMMA grafted SiO_2 increase the impact strength more effectively than untreated SiO_2. In contrast to the generally brittle–tough transition behavior in particulate filled polymeric composites, a decrease in impact strength is only observed here when the filler loading exceeds the value corresponding to the maximum impact strength. The unnotched Charpy impact tests show a similar trend (Fig. 12(a)), but even a more impressive increase in the impact strength by a factor of around 4 at a rather low filler loading (0.65 vol% for SiO_2-*g*-PS). Considering that Izod and Charpy impact tests are actually industrial testing methods, that are to some degree influenced by the specimen geometry, the SENB test, which has a more stringent theoretical basis, is better suited to characterize the toughness properties of the nanocomposites. It is seen from Fig. 12(b) that with a rise in filler content, the fracture energy, G_{IC}, first increases, and then decreases. Evidently, a higher content of grafted nanoparticles is detrimental to the impact properties and the fracture energy of the nanocomposites. The toughness improvement with the addition of modified silica should also be a result of the improved interfacial interaction in the nanocomposites owing to the interdiffusion and entanglement between the grafting polymer chains and the matrix molecules at the interfacial region. With respect to the decreasing tendency of the fracture toughness at higher filler loadings, this might be attributed to the nanoparticle clusters originating in this range (Fig. 10); they may inhibit plastic deformation of the matrix by constraining effects or simply by splitting. It is reasonable to assume that a filler content dependent competition exists between the inducing and the restricting effects of fillers on the matrix deformation, and that the trends in toughness of the nanocomposites is a function of the predominating mechanisms.

Like in the tensile tests, the effects of interfacial characteristics on the impact resistance of nanocomposites can be seen most clearly by changing the species of the grafting polymers (Table 4). For conventional particulate filled composites, poor interfacial adhesion was shown to be disadvantageous for the materials' impact property [23–25]. This is also the case for the present nanocomposites. The addition of PMA grafted silica into PP, for instance, results in an impact toughness even lower than that of the neat matrix. This is due to the specific molecular structure of

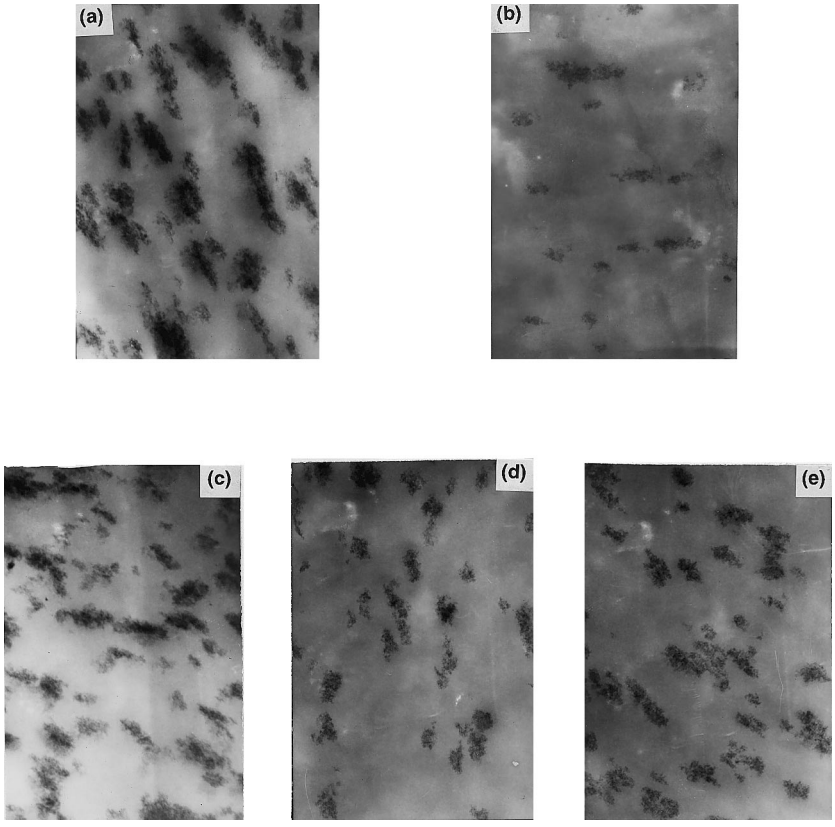

Fig. 10. TEM micrographs of PP (MI = 6.7 g/10 min) based nanocomposites filled with: (a) SiO_2 as-received (content of SiO_2 = 1.96 vol%); (b) SiO_2-*g*-PS (content of SiO_2 = 1.96 vol%); (c) SiO_2-*g*-PS (content of SiO_2 = 6.38 vol%); (d) SiO_2-*g*-PMMA (content of SiO_2 = 1.96 vol%); and (e) SiO_2-*g*-PMMA (content of SiO_2 = 6.38 vol%). Magnification = 2×10^4.

PMA. It contains carboxyl groups and prefers to react with the surface of SiO_2 (possessing hydroxyl groups) rather than entangle with the non-polar matrix. When the nanocomposites filled with SiO_2-*g*-PMA are subjected to impact loading, the weak interfacial regions are not able to resist crack propagation as effectively as the polymer matrix. Nevertheless, there are not many differences between the other grafting polymers, manifesting that a strict miscibility matching between the grafting polymers and the matrix polymer are not required, as long as a certain degree of molecular entanglement takes place.

Returning to the filler loading dependence of the nanocomposites' toughness, it should be noted here that the maxima in impact strength and fracture toughness appear already at very low filler loadings (<1–3 vol%, Fig. 12). This is opposite to the optimum loading conditions known for conventional particle filled systems. Although the typical size of the modified nanoparticles at the above-mentioned filler content range varies between 100 and 150 nm (as found by TEM observation), the distances between individual particles and therefore the interparticle ligament thicknesses are still much larger than those found

Table 4
Mechanical properties of PP (MI = 8.5 g/10 min) based nanocomposites (content of SiO_2 = 3.31 vol%) filled with different polymers grafted SiO_2 (the grafting conditions are the same as those used in Table 2)

	Nanocomposites						Neat PP
Grafting polymers	PS	PBA	PVA	PEA	PMMA	PMA	
Tensile strength (MPa)	34.1	33.3	33.0	26. 8	35.2	33.9	32.0
Young's modulus (GPa)	0.92	0.86	0.81	0.88	0.89	0.85	0.75
Elongation-to-break (%)	9.3	12.6	10.0	4.6	12.0	11.9	11.7
Area under tensile stress–strain curve (MPa)	2.4	3.3	2.3	0.8	3.2	2.9	2.2
Unnotched Charpy impact strength (kJ/m^2)	19.8	19.4	22.9	14.6	20.5	4.7	8.0

Table 5
Dependence of mechanical properties of PP (MI = 8.5 g/10 min) based nanocomposites (content of SiO_2 = 3.31 vol%) filled with SiO_2-*g*-PS (weight ratio of styrene/SiO_2 = 20/1000) on irradiation dose during pregrafting

Irradiation dose (Mrad)	Tensile strength (MPa)	Young's modulus (GPa)	Elongation-to-break (%)	Area under tensile stress–strain curve (MPa)	Unnotched Charpy impact strength (kJ/m^2)
2	36.5	0.89	11.8	3.3	37.5
10	34.1	0.92	9.3	2.4	19.8
20	33.2	0.82	8.0	2.0	3.7
Neat PP	32.0	0.75	11.7	2.2	8.0

in toughness optimized conventional particle filled systems [20]. Therefore, the considerable toughening effect perceived at such a low filler loading in the present nanocomposites implies that the mechanisms involved should be different from those used as a basis for the single percolation concept of Wu [21], which has been proved to be well applicable to conventional particulate filled polymer composites. To overcome this problem, a new, hypothetical model of double-percolation is suggested here, in which the appearance of a connected shear yielded networks is responsible for the performance enhancement at low filler loading. Its principle is based on: (a) a percolation of the shear yielded zones inside the dispersed phases (consisting of the nanoparticles, the grafted and homopolymerized polymer) due to the superposition of stress volumes around the primary particles; and (b) a percolation of the shear yielded zones throughout the matrix resin due to the superposition of stress volumes around the dispersed phases. According to the common law of scaling theory [22], such a multiple percolation process is beneficial to a low percolation threshold, i.e. a low brittle–ductile transition threshold.

Although the above proposed double-percolation model needs quantitative analysis as well as much more evidence, there are already some experimental data supporting it, including the following fractography studies (Section 3.4). Regarding the percolation inside the modified nanoparticles, the significant decrease in impact strength with increasing weight ratio of styrene to SiO_2 (Table 6), for example, can be interpreted by the fact that the stress volume fraction is reduced to a value lower than the percolation threshold. Another example is given in Table 5, showing a significant decrease in impact strength with a rise in irradiation dose. As a higher irradiation dose might induce a crosslinking structure of the grafting polymers, shear deformation of the polymers adherent to the nanoparticles becomes more difficult. Consequently, a long-range connection of the deformed polymers is hindered. In addition, Fig. 13 indicates the changes in the percentage of grafting and grafting efficiency, as induced by different preheating temperatures, do have nearly no influences on the impact strength of the nanocomposites; this leaves traces for a further investigation of the microstructure dependent toughening mechanisms.

3.4. Fractography

SEM micrographs of the fractured surfaces obtained during tensile testing of nanocomposite specimens are shown in Fig. 14. Neat PP has a relatively smooth surface and exhibits no signs of plastic deformation or drawing (Fig. 14(a)). A coarser appearance can be observed on the fractured surface of the composite containing untreated SiO_2; but it can be still characterized as semi-brittle, with only a little plastic deformation of the matrix in some regions (Fig. 14(b)). In contrast, the nanocomposite incorporating PS-grafted SiO_2 particles shows a clear evidence of plastic deformation (Fig. 14(c)). Distinct features of the fractured surface are: (1) the formation of elongated matrix segments; and (2) extensive "cavitation" sites, as indicated by a number of concentric "matrix-fibrillated" circles around particle-like objects. Magnified microphotos in Fig. 14(d) and (e)) indicate that the appearance of the fibrillated matrix circles are probably the result of a successive debonding of the modified nanoparticles from the matrix due to the interfacial stress concentrations. The latter is accompanied by an unconstrained plastic stretching of the interparticle matrix ligaments. The voiding process can be described as follows. At the beginning of the deformation, the modified nanoparticles act as stress concentrators, and the stress field is disturbed by the surrounding particles. Then shear yielding

Table 6
Dependence of mechanical properties of PP (MI = 8.5 g/10 min) based nanocomposites (content of SiO_2 = 3.31 vol%) filled with SiO_2-*g*-PS on the content of styrene during pregrafting (irradiation dose = 10 Mrad)

Weight ratio of styrene/SiO_2	Tensile strength (MPa)	Young's modulus (GPa)	Elongation-to-break (%)	Area under tensile stress–strain curve (MPa)	Unnotched Charpy impact strength (kJ/m^2)
10/100	32.9	0.83	9.9	2.8	29.5
20/100	34.1	0.92	9.3	2.4	19.8
30/100	32.7	0.84	8.7	2.1	13.6
Neat PP	32.0	0.75	11.7	2.2	8.0

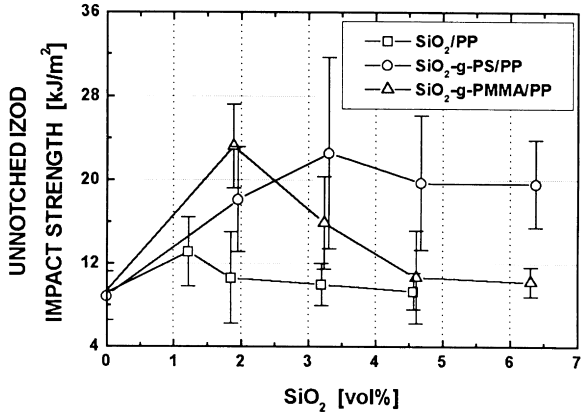

Fig. 11. Unnotched Izod impact strength of PP (MI = 8.5 g/10 min) composites filled with various nano-SiO_2 as a function of the filler loading.

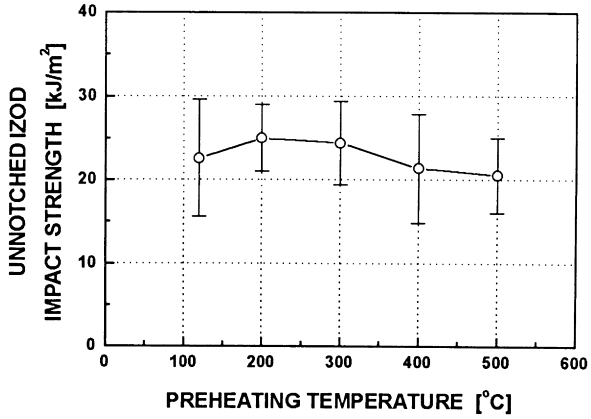

Fig. 13. Preheating temperature dependence of unnotched Izod impact strength of PP (MI = 8.5 g/10 min) based nanocomposites filled with SiO_2-*g*-PS (content of SiO_2 = 3.31 vol%).

of the matrix occurs due to a maximum shear stress component under an angle of 45° [23]. Once debonding is initiated at both ends of the modified nanoparticle agglomerates (i.e. at the poles), the shear stress is locally relieved and the deformation circles form due to a gradual contraction of the matrix. Reasonably, the presence of the concentric "fibrillar" circles around the nanoparticle agglomerations must have consumed a considerable amount of energy during the tensile procedure, which might account for the measured reinforcing and toughening effects. Fig. 14(f)–(h) represents fractured surface details of other modified SiO_2 filled PP samples. Obviously, the similarity between the fracture morphologies of these nanocomposites is consistent with their mechanical testing results.

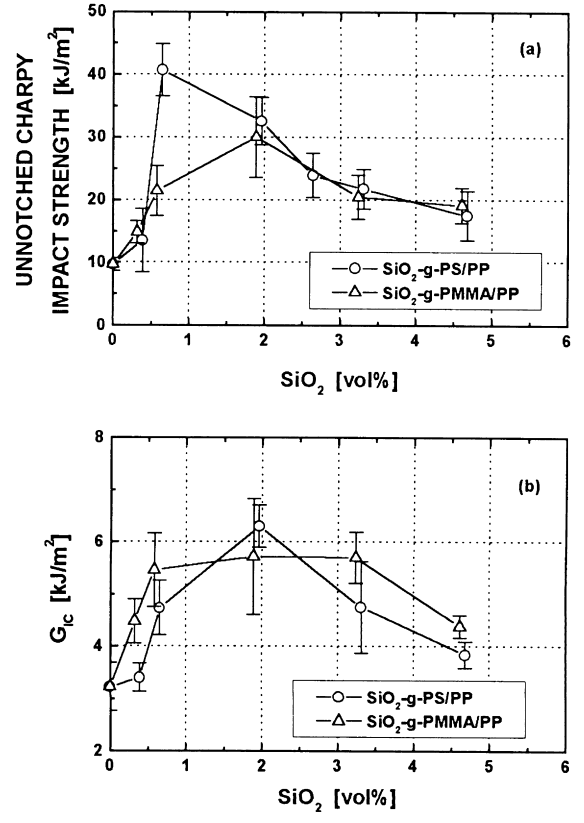

Fig. 12. Filler content dependence of: (a) unnotched Charpy impact strength; and (b) fracture toughness, G_{IC}, of PP (MI = 6.7 g/10 min) based nanocomposites filled with various nano-SiO_2.

Figs. 15 and 16 show fractured surface micrographs of specimens subjected to SENB conditions. Neat PP (Fig. 15(a) and (b)) shows again a smooth profile near the notch tip, typically indicating a brittle fracture behavior. The zone near the notch tip corresponds to the first stage of the fracture process (slow speed process) and is directly related to the toughness of PP [26]. The micrographs in Fig. 16(a)–(c) demonstrate that for the nanocomposite with only 0.39 vol% PS-grafted SiO_2, the overall fracture is semi-brittle in nature, but already with a limited area of plastic deformation near the notch tip. Circular fibrillation and microvoids, similar to the cavities and shear yielding circles found on the tensile fractured surfaces (Fig. 14), can also be found here on the photos with higher magnification (Fig. 16(b) and (c)). Nevertheless, only a slight increase in G_{IC} (as compared to that of neat PP) could be detected at this composition (Fig. 12(b)). Corresponding to the maximum G_{IC} value of SiO_2-*g*-PS/PP given in Fig. 12(b) (ca. 2 vol% SiO_2), these fractured surfaces are accompanied by extensive plastic deformation and a number of concentric fibrillar circles (Fig. 16(d)–(f)). It is noteworthy that these circles have overlapped and pervaded over the entire matrix in the deformation zone, which is actually an indication of the percolation behavior induced by the modified nanoparticles. In this way, the yielding process of the matrix propagates through the ligaments between the dispersed phases, in which a plain-strain to plain-stress transition takes place accordingly.

It should be mentioned, however, that the relatively low G_{IC} of the nanocomposites with 4.68 vol% SiO_2-*g*-PS cannot be explained by the SEM fractographs (Fig. 16(g)–(i)). In this case, also many extensive plastic deformation sites and connected yielding circles can be observed.

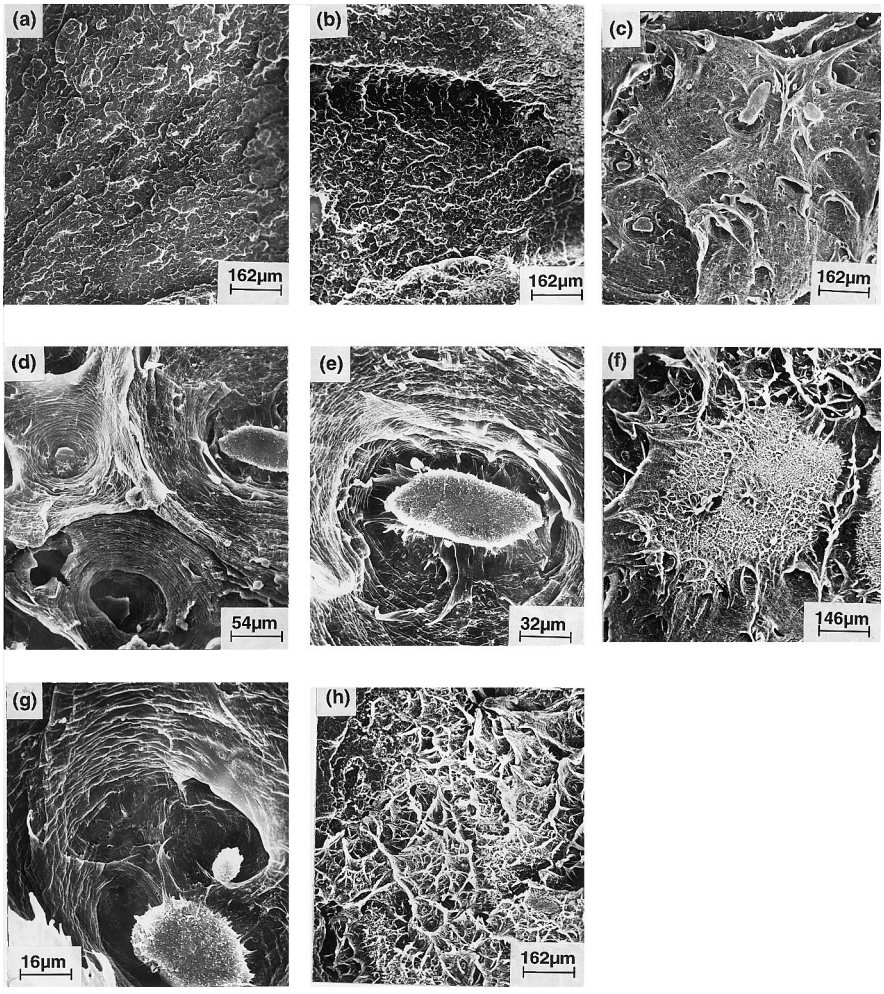

Fig. 14. SEM fractographs of tensile fractured surface of: (a) neat PP (MI = 6.7 g/10 min); (b) SiO_2 as-received/PP (content of SiO_2 = 1.33 vol%); (c)–(e) SiO_2-*g*-PS/PP (content of SiO_2 = 1.96 vol%); (f) and (g) SiO_2-*g*-PMMA/PP (content of SiO_2 = 1.96 vol%); (h) SiO_2-*g*-PBA/PP (content of SiO_2 = 3.31 vol%).

However, by a careful comparison between Fig. 16(f) and (i), it seems that the former has undergone a stronger plastic deformation characterized by more wrinkle-like patterns on the matrix around the modified nanoparticle agglomerates. That means, the deleterious effect of a higher filler content on the toughness of the nanocomposite might be a result of a restriction in matrix deformation.

3.5. Effect of modified nanoparticles on the crystallization characteristics of PP

The improvement of the mechanical properties of PP by the addition of modified nanoparticles was discussed in the above sections. It is still unclear, however, whether the microstructure of the PP matrix was influenced by these particles, since this might in turn, affect the performance of the nanocomposites studied here. As PP is a semicrystalline polymer, having properties that are strongly related to its crystalline characteristics, DSC studies of its non-isothermal crystallization and melting behavior are of great interest (Table 7). The experimental data demonstrate that both, untreated and PS-grafted SiO_2 particles, have some nucleation influence on the crystallinity of the PP even within a small temperature range of less than 1°C. In fact, the supercooling temperature, ΔT, of the nanocomposites decreases with increasing filler content for both untreated and PS-grafted SiO_2 filled systems, indicating that the crystallization becomes easier in the nanocomposites due to the nucleation effect of the fillers. On the other hand, the results show that the crystallinity and melting point of PP are not significantly affected by the addition of the fillers, e.g. the difference between the untreated SiO_2 and the PS-grafted SiO_2 filled system could not be detected during the current non-isothermal crystallization measurements.

Table 8 shows the kinetic parameters of the isothermal crystallization of the neat PP and its nanocomposites at 130 and 132°C, respectively. It is evident that the systems with fillers have shorter crystallization times including $t_{1/2}$, t_{max} and t_f, and greater crystallization rate constant, K, in comparison to the neat PP. This suggests that the

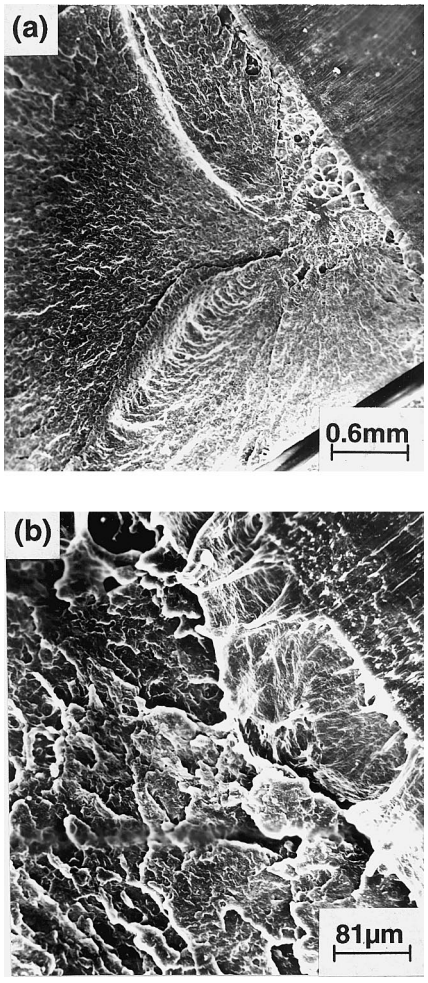

Fig. 15. SEM fractographs of SENB fractured surface near the notch tip of neat PP (MI = 6.7 g/10 min).

crystallization rate of PP is increased by the nucleation effect of the fillers. As the values of $t_{1/2}$, t_{max} and t_f of untreated SiO_2/PP are the lowest, it becomes obvious that the nucleation effect of the untreated SiO_2 is more profound than that of the other polymer grafted SiO_2 particles. This is imaginable because in the systems containing modified SiO_2 the contacts between SiO_2 and the matrix is reduced by the grafting polymers. All the kinetic parameters of isothermal crystallization reported here for the modified SiO_2 filled PP are in full agreement with those of the core-shell structural elastomer/inorganic particles/matrix ternary system [14]. On the other hand, the data of both the crystallization enthalpy and the melting temperature of the nanocomposites, remained almost the same as those measured for the neat PP (Table 8).

On the basis of both the non-isothermal and isothermal DSC measurements, it can be concluded that the crystalline features of the matrix have not been influenced greatly by the addition of the fillers, even though the fillers exert some nucleation effect on the crystallization of the PP matrix. Due to the fact that the untreated SiO_2, exhibiting a slightly more significant nucleation effect, could not improve the mechanical properties of PP equivalently, it is believed that the reinforcing and toughening effects of the modified nanoparticles are brought into play only through a change of the stress state around the fillers.

4. Conclusions

In the present study, various polymers were grafted on the surface of nano-scale silica filler particles through the simultaneous irradiation polymerization technique. It was confirmed that the polymer chains were chemically bonded to the fillers. In addition, the modification method was more simple and much easier to carry out because the nanoparticles possessed a higher reactivity in comparison to conventional micron-scale inorganic particles. This means that the modified nanoparticles can be more effectively utilized in thermoplastics than conventional particulate fillers, when using the same direct compounding technology. Some reasons for this are listed below:

Firstly, the significant increase in the hydrophobicity of the nanoparticles due to the presence of the grafting polymers is beneficial for the filler/matrix miscibility, even though the fillers could not be dispersed completely in the form of primary nanoparticles in the polymer matrix.

Secondly, the filler/matrix interaction is substantially enhanced by the entanglement of the grafting polymers and the matrix polymer.

Thirdly, the nanoparticle agglomerates become much stronger, and in addition, the direct contacts between the particles no longer appear because of the uniform coverage of grafting polymers on the surface of each nanoparticle.

As a result of these phenomena, reinforcing and toughening effects of the nanoparticles on polymeric materials could be fully brought into play. In fact, the tensile properties, such as strength, modulus and elongation at break of PP were improved simultaneously when the modified nanoparticles were incorporated. This is hard to find in conventional particulate composites. By changing the species of the grafting monomers, the tensile properties of the nanocomposites could also be purposely adjusted according to their interfacial viscoelastic properties. It was also found that the internal structure of the modified nanoparticles had an additional influence on the mechanical properties of the nanocomposites. For example, the optimum nanoparticle content was related to the optimum distribution of the particles. With respect to the impact resistance and fracture toughness of the nanocomposites, a considerable toughening effect could be observed at a rather low loading of the modified fillers. This was temporarily interpreted by a hypothetical model, taking into account the double-percolation mechanisms of stress volumes inside and around the dispersed phases.

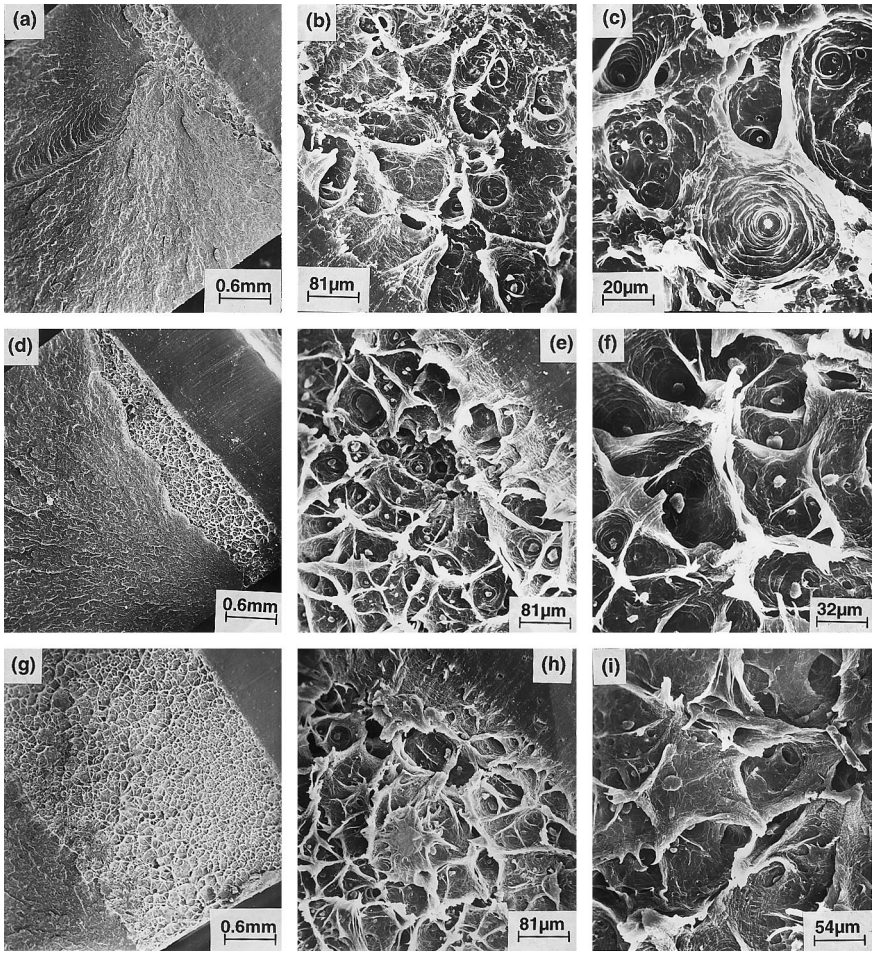

Fig. 16. SEM fractographs of SENB fractured surface near the notch tip of PP (MI = 6.7 g/10 min) based nanocomposites filled with SiO_2-*g*-PS. SiO_2 content: (a)–(c) 0.39 vol%; (d)–(f) 1.96 vol%; (g)–(i) 4.68 vol%.

Table 7
Non-isothermal crystallization and melting data of PP (MI = 8.5 g/10 min) and its nanocomposites

Samples	Content of SiO_2 (vol%)	T_m[a] (°C)	T_{cn}[b] (°C)	ΔT[c] (°C)	X_c[d] (%)
Neat PP	–	164.7	115.3	49.4	44.6
Nanocomposites filled with untreated SiO_2	1.96	165.8	117.8	48.0	46.4
	3.31	166.6	118.9	47.7	45.1
	4.68	164.4	118.6	45.8	44.4
	6.38	163.3	118.9	44.4	46.7
Nanocomposites filled with SiO_2-*g*-PS	1.96	164.7	116.5	48.2	45.8
	3.31	166.2	118.9	47.3	43.9
	4.68	164.9	118.7	46.2	46.9
	6.38	165.3	119.1	45.3	44.6

[a] T_m denotes the peak melting temperature.
[b] T_{cn} denotes the peak crystallization temperature recorded during cooling.
[c] $\Delta T = T_m - T_c$, denotes the supercooled temperature.
[d] X_c denotes the crystallinity of PP.

Table 8
Kinetic parameters of isothermal crystallization of neat PP (MI = 8.5 g/10 min) and its nanocomposites

Samples	T_{ci}[a] (°C)	ΔH[b] (J/g)	t_f[c] (min)	t_{max}[d] (min)	$t_{1/2}$[e] (min)	n[f]	K[g] (min^{-n})	T_m (°C)
Neat PP	130	95.6	14.6	5.7	6.1	2.69	5.30×10^{-3}	166.5
	132	97.9	23.8	9.8	10.1	2.75	1.18×10^{-3}	167.1
SiO_2 as-received/PP[h]	130	92.3	10.2	4.1	4.3	3.10	7.16×10^{-3}	166.8
	132	94.7	17.1	7.5	7.9	2.94	1.64×10^{-3}	167.3
SiO_2-*g*-PS/PP[h]	130	93.4	11.3	4.9	5.0	2.84	7.15×10^{-3}	168.6
	132	95.2	18.7	8.9	8.8	2.99	1.07×10^{-3}	167.2
SiO_2-*g*-PMMA/PP[i]	130	94.6	12.4	5.1	5.2	3.02	5.87×10^{-3}	167.0
	132	94.0	18.2	7.7	8.1	2.80	1.98×10^{-3}	168.0

[a] T_{ci} denotes the present isothermal crystallization temperature.
[b] ΔH denotes the enthalpy of crystallization.
[c] t_f denotes the time at which the crystallization is completed.
[d] t_{max} denotes the time at which the crystallization rate is the maximum.
[e] $t_{1/2}$ denotes the time at which the crystallization is carried out for a half.
[f] n denotes the Avrami index.
[g] K denotes the rate constant of crystallization.
[h] Content of SiO_2 = 3.31 vol%.
[i] Content of SiO_2 = 1.96 vol%.

It is worth noting that the current irradiation grafting modification method has been proved to be very effective in improving the strength and toughness of thermoplastics with the addition of only a small amount of modified inorganic nanoparticles (typically less than 3% by volume). Further studies are necessary to generate information about other advantages of these nanocomposites compared to other conventional particulate filled polymeric composites, e.g. with regard to a lower processing viscosity (Fig. 17), or transparent and lower density of products.

Further studies should be made to identify the internal structure of the modified nanoparticle agglomerates and the distribution details of the particles in the matrix, viscoelastic characteristics of interphase, and crystallization feature in the layer nearing the fillers.

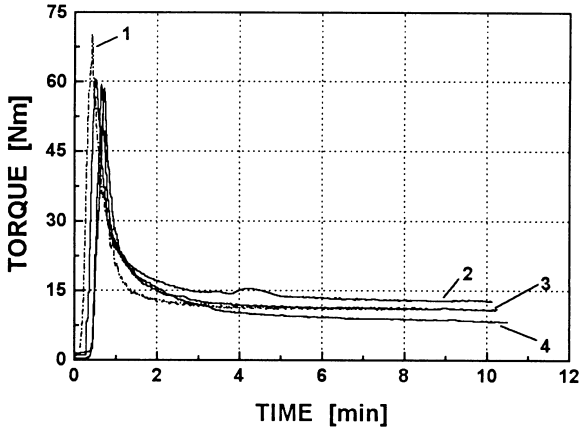

Fig. 17. The torque–time curves of: (1) PP (MI = 8.5 g/10 min); (2) SiO_2-*g*-PS/PP; (3) SiO_2-*g*-PMMA/PP; and (4) SiO_2 as-received/PP. SiO_2 content = 3.31 vol%.

Acknowledgements

The financial support by the Natural Science Foundation of China (Grant: 59725307), the Deutsche Forschungsgemeinschaft (DFG FR675/34-1), the Foundation for the Excellent Youth Scholars of the Ministry of Education of China, the Key Programs of the Ministry of Education of China (Grant: 98069, 99198), and the Natural Science Foundation of Guangdong (Grant: 990277) are gratefully acknowledged. Dr M. Rong is grateful to the support of the Pilot Program for Young PhD of the Natural Science Foundation of Guangdong (no. 974072).

References

[1] Pukanszky B. Particulate filled polypropylene composites. In: Karger-Kocsis J, editor. Polypropylene: an A–Z reference, Dordrecht: Kluwer Academic Publishers, 1999. p. 574–80.
[2] Savadori A, Scapin M, Walter R. Macromol Symp 1996;108:1–289.
[3] Dagni R. C&EN 1992;23:18–24.
[4] Novak BM. Adv Mater 1993;5(6):422–33.
[5] Giannelis EP. Adv Mater 1996;8(1):29–35.
[6] Xu W, Huang R, Cai B, Fan W. China Plastics 1998;12(6):30–4.
[7] Sumita M, Tsukumo Y, Miyasaka K, Ishikawa K. J Mater Sci 1983;18:1758–64.
[8] Li JX, Silverstein M, Hiltner A, Baer E. J Appl Polym Sci 1994;52:255–67.
[9] Ess JW, Hornsby PR. Plast, Rubber Compos Process Appl 1987;8:147–56.
[10] Wang Y, Huang JS. J Appl Polym Sci. 1996;60:1779–91.

[11] Fukano K, Kageyama E. J Polym Sci, Polym Chem Ed 1976;14:1743–51.
[12] Sahnoune F, Lopez-Cuesta JM, Crespy A. J Mater Sci 1999;34:535–44.
[13] Long Y, Shanks RA. J Appl Polym Sci 1996;61:1877–85.
[14] Long Y, Shanks RA. J Appl Polym Sci 1996;62:639–46.
[15] Pukanszky B. Composites 1990;21:255–62.
[16] Quazi RT, Bhattacharya SN, Kosior E. J Mater Sci 1999;34:607–14.
[17] Demjen Z, Pukanszky B. Polym Comps 1997;18:741–7.
[18] Kendall K, Sherliker FR. Br Polym J 1980;12:111–3.
[19] Walter R, Friedrich K, Privalko V, Savadori A. J Adhes 1997;64:87–109.
[20] Fu Q, Wang G. Polym Int 1993;30:309–12.
[21] Wu S. Polymer 1985;26:1855–63.
[22] Zallen R. The physics of amorphous solids. New York: Wiley, 1983.
[23] Kim GM, Michler GH, Gahleitner MF. J Appl Polym Sci 1996;60:1391–403.
[24] Friedrich K, Karsch UK. J Mater Sci 1981;16:2167–75.
[25] Tjong SC, Li RKY, Cheung T. Polym Engng Sci 1997;37:166–72.
[26] Bramuzzo M, Savadori A, Bacci D. Polym Comps 1985;6:1–8.